THE ASTROPHYSICAL JOURNAL, 446:759–765, 1995 June 20

THE WEAKENING OF THE TERMINATION SHOCKS OF ISOTHERMAL WINDS BY MASS LOADING

R. J. R. WILLIAMS,[1] T. W. HARTQUIST,[2] AND J. E. DYSON[1]
Received 1994 September 14; accepted 1994 December 29

ABSTRACT

An analysis of the dynamics of supersonic mass-loaded isothermal winds shows that in many situations such a wind will pass through one or more global shocks at speeds much lower than the wind's maximum velocity. A method for estimating the Mach number of the global shock in a mass-loaded, spherically symmetric, isothermal wind is given. The criteria that must be met for the assumption that the wind is isothermal to be valid are treated. We discuss the asymptotic behavior of these winds and the nature of sonic points in them. Numerical solutions for the Mach numbers of isothermal winds for different radial dependences of the mass-loading rate are given. The possible relevance of low shock speeds in some mass-loaded isothermal winds for radio quietness is mentioned.

Subject headings: hydrodynamics — radio continuum: general — shock waves

1. INTRODUCTION

The observed properties of bubbles blown by the winds of highly evolved stars (e.g., Smith et al. 1984; Meaburn et al. 1991) have led to the conclusion that the structures and evolution of the bubbles are greatly affected by the interactions of the winds with clumps of stellar material ejected during prior stages of mass loss (Smith et al. 1984; Hartquist et al. 1986; Meaburn et al. 1991; Dyson & Hartquist 1992; Hartquist & Dyson 1993). Consequently, detailed one-dimensional, time-dependent hydrodynamic models of specific wind-blown bubbles associated with evolved stars have been constructed (Arthur, Dyson, & Hartquist 1993, 1994). The nature of winds mass-loaded by the ablation of and evaporation of material from embedded clumps (or stellar sources) has also received theoretical attention in the context of galactic winds (Mathews & Baker 1971), globular cluster winds (Durisen & Burns 1981), starburst galaxy superwinds (Chevalier & Clegg 1985; Leitherer 1994 and reference therein), accretion flow-wind structures at the centers of active galactic nuclei (Beltrametti & Perry 1980; David, Durisen, & Cohn 1987a, b; Williams 1993; Poll 1994), and ultracompact H II regions (Dyson & Williams 1995). Some general properties of steady, mass-loaded, adiabatic winds have recently been examined by Smith (1994).

The work of Arthur et al. (1994) showed that in at least some isothermal mass-loaded winds, a global shock does not occur in the region where the Mach number is large. Instead, the wind passes through a global shock only after it has traveled far enough for mass loading to decelerate it sufficiently that its Mach number is less than a few. In some of these cases, a global shock within the mass-loading region does not exist at all, but a termination shock caused by the interaction of the wind with an external ambient medium is located beyond the mass-loading region; obviously, in such a case, mass-loading of the wind reduces its speed at this termination shock.

Wendker et al. (1975) have noted that though IC 443, a supernova remnant, and NGC 6888, a Wolf-Rayet stellar wind–blown bubble, show some similarities, they differ significantly from one another in their radio properties. While IC 443 is a very strong nonthermal radio source, NGC 6888's radio emission is completely thermal in origin. That stellar wind-blown bubbles usually are not synchrotron sources is so widely accepted by now that the presence of nonthermal radio emission is sometimes cited as evidence that an object is not a stellar wind–blown bubble (e.g., Bally et al. 1989; Kulkarni et al. 1992).

The gradual deceleration of a wind by mass-loading and the associated weakening of the shock may in fact contribute to the radio quietness of some wind-blown bubbles. This is a conjecture which currently cannot be proven because, whereas heavier cosmic-ray particles apparently may be injected from the suprathermal tails of their momentum distributions in an immediate postshock plasma (e.g., Ellison & Möbius 1987), the mechanism by which cosmic-ray electrons are injected remains unknown as does the mechanism by which electrons are heated in collisionless shocks (e.g., Asvarov 1992). However, the conjecture is reasonable if the fraction of injected electrons is independent of the shock speed, but the typical injection energy per electron is proportional to the postshock temperature; then a smaller percentage of the electrons behind a slower shock would reach the roughly GeV energies associated with the cosmic-ray electrons that emit the observed synchrotron radiation. For this conjecture to be valid, the entrainment of clump material into the wind must be primarily through gradual viscous coupling between the wind and the entrained material, and only a small fraction of the wind may pass at high velocity through those sections of bow shock surfaces that have normals with significant components parallel to the wind velocity; we do not consider the question of flow structure on these intermediate scales which are associated with entrainment but will address it in future work.

The main aim of the work presented in this paper is the calculation of the Mach numbers of the global shocks in isothermal mass-loaded winds. The results may be of relevance to the nonthermal radio quietness of some sources, but they certainly bear on the issue of the thermal emission of wind-blown bubbles. For instance, the absence of a high Mach number global shock in a mass-loaded wind leads the bubble to be a

[1] Department of Physics and Astronomy, University of Manchester, M13 9PL, UK.
[2] Max-Planck-Institut für extraterrestrische Physik, 85740 Garching, Germany.

weaker X-ray source than a bubble blown by a comparable wind that develops a high Mach number global shock.

Section 2 contains estimates of the locations and Mach numbers of shocks in spherically symmetric mass-loaded isothermal winds. In § 3, we give criteria for the validity of the assumption of isothermal flow, while § 4 concerns the properties of the sonic points in spherically symmetric, steady, mass-loaded isothermal winds and the flow structures at large radii in infinitely extended mass-loading regions. Section 5 gives numerical solutions for the wind Mach number as a function of radius for infinitely extended mass-loaded regions in which the mass-loading rate has various radial dependences; the section also has numerical results for finite mass-loading zones and the Mach number of shocks occurring in them. Section 6 is a brief conclusion.

2. APPROXIMATIONS TO THE SHOCK LOCATION AND SHOCK MACH NUMBER

We consider a steady isothermal wind flowing radially through a spherically symmetric mass-loading region which extends to radius r_L and is centered on the source of the wind. We assume that mass-loading smoothly decelerates the wind until is passes through a global shock at radius r_s (we will see below that r_s must be less than r_L), and that the mass-loaded wind remains subsonic to radius r_P (where $r_s < r_P \leq r_L$), at which it passes smoothly through a sonic point to become supersonic again. Related approximations have been used in the case of combined wind-accretion flows by Ostriker et al. (1976) and Durisen & Burns (1981).

We consider the case of a mass-loaded wind with no gravitational forces, which leads to considerable simplifications in the analysis. Gravitational effects are small, so long as the wind driven from small radii is supersonic when it reaches the region in which mass-loading is important. This is likely to be true for most nebulae around stars. For example, around the nucleus of a planetary nebula $2GM_*/c^2 \lesssim 10^{15}$ cm (where the limit corresponds to $M_* \simeq 10\ M_\odot$ and $c \simeq 15$ km s^{-1}), far smaller than the PN radius. Close to this radius, radiative forces are also likely to have an important effect. We neglect both gravity and these radiative forces and assume that the flow from small radii is highly supersonic and can be specified by a central mass-loss rate $\dot{M}_*$ and velocity v_*.

The values of $\dot{M}_*$ and v_* are determined by gravitational and radiative forces close to the star and match the solutions in the mass-loading region at some small but finite radius $r > r_*$ where these forces have become negligible. These values are well defined if the stagnation pressure of the stellar wind flow at the sonic point close to the stellar surface is far larger than that in the mass-loading region, or in the surrounding ambient interstellar medium (ISM).

The dynamics of the wind are governed by the equation of continuity

$$\frac{d}{dr}(\rho v r^2) = S r^2 , \tag{1a}$$

and the force equation

$$\frac{1}{r^2}\frac{d}{dr}(\rho v^2 r^2) = -\frac{dP}{dr} , \tag{1b}$$

where r is the distance from the wind source; v and ρ are, respectively, the wind speed and density; and P is the pressure. S is the rate per unit volume at which mass is entrained by the wind. In isothermal flow

$$P = \rho c^2 , \tag{1c}$$

where c is the isothermal sound speed. Equation (1) integrates to give

$$\dot{M}(r) \equiv 4\pi r^2 \rho v = \dot{M}_* + I(r) , \tag{2a}$$

where

$$I(r) \equiv 4\pi \int_{r_*}^{r} S r^2\, dr , \tag{2b}$$

and $\dot{M}_*$ is the mass-loss rate of the central source, at its surface $r = r_*$.

To estimate the global shock radius r_s, we balance the ram pressures of preshock and postshock flow. We first estimate the ram pressure of the supersonic wind at a radius only marginally less than r_s. Use of equations (1a), (1b), and (1c) yields

$$(v^2 - c^2)\frac{dv}{dr} = -\frac{S}{\rho}(v^2 + c^2) + \frac{2vc^2}{r} . \tag{3}$$

If we assume that the flow is hypersonic at $r < r_s$, we obtain

$$\frac{dv}{dr} \simeq -\frac{S}{\rho} . \tag{4a}$$

Use of the relation (2a) permits us to eliminate ρ from equation (4a) and then to integrate to find that

$$v \simeq \frac{v_*}{1 + [I(r)/\dot{M}_*]} , \tag{4b}$$

where v_* is the speed of the wind at small r. Employing equations (2a) and (4b), we find that the ram pressure of the mass-loaded supersonic wind at r_s is roughly

$$P_s \simeq \frac{\dot{M}_* v_*}{4\pi r_s^2} . \tag{5}$$

We next calculate the sum of the ram pressure and the thermal pressure at the sonic radius, r_P. This is the radius at which $v = c$, so for a solution to exist, the right-hand side of equation (3) must also vanish. In the case of an isolated, spherically symmetric mass loading region, sonic points where the flow becomes supersonic can either occur within the region (for particular mass-loading distributions, see below), or can be "synthesized" at its edge ($r_L = r_P$) if the forms of the steady solutions within and outside the region are suitable (cf. Fig. 2; Chevalier & Clegg 1985; Williams & Dyson 1994).

In this paper, we assume that the wind from the nebula has driven the ambient ISM to radii well beyond the mass-loading region, so the flow in this region can be treated as steady. The influence of the ISM can be included as a boundary condition on the pressure at infinity, P_∞, for these steady flows (cf. Parker 1965). The flow must be supersonic beyond the mass-loading region for sufficiently low external pressure ($P_\infty \lesssim P_P$). A shock at some intermediate radius will then match the *fully determined* transonic solution with the nebula to the external pressure. This is the more likely case, which we treat here. Alternatively, if $P_\infty \gtrsim P_P$, the external pressure will stagnate the flow onto a breeze solution, which is everywhere subsonic beyond the inner shock radius. The stagnation pressure of the

breeze solutions is finite at infinity: the external ISM pressure will determine which breeze solution is appropriate; the inner shock will be driven to radii rather smaller than those found for the transonic solution.

Using the fact that $v = c$ at r_P, and equations (1c) and (2a), we find that the sum is

$$P_P = \frac{[\dot{M}_* + I(r_P)]c}{2\pi r_P^2} . \tag{6}$$

Because by assumption the flow between r_s and r_P is subsonic, to a good approximation

$$P_s \simeq P_P , \tag{7a}$$

from which we find that

$$r_s \simeq \left\{\frac{\dot{M}_* v_*}{2[\dot{M}_* + I(r_P)]c}\right\}^{1/2} r_P . \tag{7b}$$

If this equation yields a value for r_s larger than r_P, then the central wind has sufficient momentum flux to drive through the whole mass-loading region, nowhere becoming subsonic: no global shock will form in the mass-loading region.

The Mach number of the shock, defined as $m \equiv v/c$, may be calculated from equations (2b), (4b), and (7b). To make this calculation, we assume that

$$I(r) = \begin{cases} \dot{M}_*\left(\dfrac{r}{r_0}\right)^{\Gamma+3} & r < r_L \\ \dot{M}_*\left(\dfrac{r_L}{r_0}\right)^{\Gamma+3} & r \geq r_L \end{cases} , \tag{8}$$

where Γ is a constant and r_0 has obviously been chosen to satisfy $I(r_0) = \dot{M}_*$. We require $\Gamma > -3$ and neglect terms of order $(r_*/r_0)^{\Gamma+3}$ required by the definition (2b). All sonic points in the flow must be inside the mass-loading sphere, so $r_P \leq r_L$. Thus from equation (4b), the shock Mach number is

$$m_s = \frac{v_*}{c}\left[1 + \left(\frac{r_s}{r_0}\right)^{\Gamma+3}\right]^{-1} \tag{9a}$$

$$\simeq \frac{v_*}{c}\left[1 + \left\{\frac{v_*(r_P/r_0)^2}{2c[1 + (r_P/r_0)^{\Gamma+3}]}\right\}^{(\Gamma+3)/2}\right]^{-1} . \tag{9b}$$

If a global shock is to form within the mass-loading region for an initially hypersonic wind, equation (7b) implies that

$$I(r_P) \gg \dot{M}_* \tag{10}$$

(and so, from eq. [8], $[r_P/r_0]^{\Gamma+3} \gg 1$). With this condition, we find from equation (9b) that

$$m_s \simeq \frac{v_*}{c}\left\{1 + \left[\frac{v_*}{2c}\left(\frac{r_P}{r_0}\right)^{-(\Gamma+1)}\right]^{(\Gamma+3)/2}\right\}^{-1} . \tag{11a}$$

Using equations (8) to substitute for (r_P/r_0) in this, we find

$$m_s \simeq \frac{v_*}{c}\left\{1 + \left(\frac{v_*}{2c}\right)^{(\Gamma+3)/2}\left[\frac{I(r_P)}{\dot{M}_*}\right]^{-(\Gamma+1)/2}\right\}^{-1} . \tag{11b}$$

From equation (11b) we see that a large reduction of m_s below v_*/c occurs if

$$\frac{v_*}{c} \gg 2\left[\frac{I(r_P)}{\dot{M}_*}\right]^{(\Gamma+1)/(\Gamma+3)} . \tag{12}$$

For the particular case $\Gamma = -2$, equations (11b) and (12) give, respectively,

$$m_s \simeq \frac{v_*}{c}\left\{1 + \left(\frac{v_*}{2c}\right)^{1/2}\left[\frac{I(r_P)}{\dot{M}_*}\right]^{1/2}\right\}^{-1} \tag{13a}$$

and

$$\frac{I(r_P)}{\dot{M}_*} \gg \frac{2c}{v_*} . \tag{13b}$$

A global shock will form in an isothermal mass-loaded wind when condition (10) holds and will have a Mach number much less than v_*/c if condition (12) is met. For $v_*/c \gg 1$ and $\Gamma \lesssim -1$, condition (10) is the more restrictive of the two; condition (10) states only that at the outer edge of the mass-loading region the flux of entrained mass must be much greater than the flux of mass that is injected by the central source. For $\Gamma \gtrsim -1$, condition (12) is more restrictive than condition (10)—any shock which forms will have an upstream Mach number substantially below that of the initial stellar wind.

3. THE ASSUMPTION OF ISOTHERMAL FLOW

We now consider conditions that must hold in order for the wind to behave isothermally while it is hypersonic. The equation for energy conservation for a $\gamma = 5/3$ gas is

$$\frac{1}{r^2}\frac{d}{dr}\left[r^2 v\left(\frac{1}{2}\rho v^2 + \frac{5}{2}P\right)\right] = H - \Lambda , \tag{14}$$

where H is the heating rate per unit volume due to processes other than mass-loading, which we assume does not add energy to the wind, and Λ is the cooling rate per unit volume. From equations (1a) and (1b) we obtain an equation governing P/ρ:

$$\frac{d\ln(P/\rho)}{dr} = -\frac{4}{3r} + \frac{1}{3}\frac{Sv}{P} - \frac{S}{\rho v} + \frac{2}{3}\frac{H-\Lambda}{vP} - \frac{2}{3v}\left(v^2 - \frac{5}{3}\frac{P}{\rho}\right)^{-1}\left(\frac{10}{3}\frac{vP}{r\rho} - \frac{4}{3}\frac{v^2 S}{\rho} - \frac{2}{3}\frac{H-\Lambda}{\rho}\right) . \tag{15}$$

If we assume that the wind is hypersonic, we need to retain only the first, second, and fourth terms on the right-hand side of equation (15). The derivative on the left-hand side of equation (15) and the first term on the right-hand side may be neglected if

$$r \gg \frac{4P}{Sv} \tag{16a}$$

and either

$$r \gg \frac{2Pv}{|H - \Lambda|} \tag{16b}$$

or

$$r \gg \frac{2Pv}{|\Lambda|} . \tag{16c}$$

If conditions (16a) and either (16b) or (16c) are met, a hypersonic wind will have a temperature given by the solution of

$$\Lambda = \tfrac{1}{2}Sv^2 + H . \tag{17}$$

If the wind remains almost fully ionized, the temperature will then vary little so long as either

$$\left|\frac{d\ln|H-\Lambda|}{d\ln T}\right|^{-1}\left|\frac{d\ln(Sv^2)}{d\ln r}\right| \ll 1 \tag{18a}$$

or

$$|H| \gg \tfrac{1}{2}Sv^2 . \tag{18b}$$

If we use equations (8), (2b), and (4b) as well as assume that $I(r) \gg \dot{M}_*$ then condition (18a) becomes

$$\left|\frac{d\ln|H-\Lambda|}{d\ln T}\right|^{-1}|\Gamma+3| \ll 1 . \tag{19}$$

For the hypersonic part of the flow to remain roughly isothermal, conditions (16a), (16b) or (16c), and (18a) or (18b) must be met.

A corresponding set of conditions is relevant to the issue of whether the flow remains isothermal in the subsonic region.

4. SOME PROPERTIES OF STEADY ISOTHERMAL MASS-LOADED FLOWS

In this section we consider the natures of sonic points in mass-loading regions and the asymptotic behavior at large r of winds in very extended mass loading regions.

From equations (1a), (1b), (1c), (8), and the definition of the Mach number, it follows that

$$\frac{x(m^2-I)}{m}\frac{dm}{dx} = 2 - \frac{\Gamma+3}{1+x^{-(\Gamma+3)}}(m^2+1) , \tag{20a}$$

with

$$x \equiv \frac{r}{r_0} . \tag{20b}$$

The solutions of this equation can have a finite gradient at Mach number of unity only at the set of sonic points where the right-hand side of the equation is zero when $|m| = 1$, that is at x_P, where

$$x_P = (\Gamma+2)^{-1/(\Gamma+3)} . \tag{21}$$

To study the nature of the flow close to these sonic points, we expand equation (20a) using l'Hôpital's rule (cf. Holzer 1977). Close to $m = 1$, we find the gradients of the solutions through a sonic point satisfy

$$x^2\left(\frac{dm}{dx}\right)^2 + x\frac{dm}{dx} + \Gamma + 2 = 0 . \tag{22}$$

The roots of this equation determine the form of the sonic point. For the narrow range $-2 \le \Gamma \le -(7/4)$ the roots are real and of the same sign and the sonic point is a node. The solutions corresponding to either of these roots can take the flow from supersonic to subsonic motion. For $\Gamma > -(7/4)$ the roots are complex, and $m(r)$ spirals in the vicinity of the sonic point; thus, for $\Gamma > -(7/4)$, a shock must exist in a steady flow for it to pass through all radii. Depending on the global form of the solutions, it is possible that a shock may also be required when the sonic point is a node. Note that an equivalent equation to (22) holds in the neighborhood of the sonic points in adiabatic flows, and there are thus similar regimes of flow topology (cf. Smith 1994).

Equation (22) holds for general mass-loading distributions, with the local value of $\Gamma(r) \equiv d\ln S/d\ln r$; the sign of the second term is reversed for inward flows, where $m \simeq -1$ (eq. [20a] does not, however, hold if Γ varies). Indeed, at some radius Γ must break to a slope steeper than -3 if the total mass loading is to be finite. For a general mass-loading distribution, it is possible that at the sonic point $\Gamma < -2$, so the roots are of opposite sign and the sonic point is a saddle. The "synthetic" sonic points discussed above and illustrated in the next section are a limit of this case, where $\Gamma \to -\infty$ suddenly at the edge of the mass-loading region.

5. NUMERICAL SOLUTIONS

Figure 1 shows solutions of equations (20a) for the Mach number as a function of radius for different values of Γ. The mass-loading regions are assumed to extend from $r_* = 0$ to infinity. For $\Gamma = 0$, the solutions form a tightly wound spiral. For $\Gamma = -1.5$, the spiral is far looser, but for either case, any flow that passes from supersonic to subsonic must go through a shock. For $\Gamma = -1.9$, however, the sonic point is a node. As the solutions approach the sonic point they are seen to be strongly attracted toward a curve that passes through it with a small gradient; this is the *nonsingular solution.* The *singular solution* is the boundary between solutions that approach the sonic point from the left and solutions that approach the sonic point from the right; it has a steeper negative gradient than the nonsingular solution. The gradients of these two solutions through the sonic point are given by equation (22) (or equivalent). Any of the upstream solutions with Mach numbers less than the singular solution can pass smoothly through the sonic point and be continued by any of the downstream subsonic solutions that have larger Mach numbers than the singular solution. For an upstream solution with higher Mach number than the singular solution to become subsonic, it must pass through a shock.

In Figures 2 and 3 we present numerical results for m in cases where the mass loading region is of finite extent. Figure 2 is for $\Gamma = 0$ and $r_L = 4r_0$. The bold curves show the unique solution that is subsonic at $r < r_L$ and transonic at $r = r_L$, and that which is supersonic at $r < r_L$ and transonic at $r = r_L$. The intersection of the dashed curve with a solution shown in Figure 2 gives the location and Mach number of the shock that connects the intersected solution (through the isothermal shock jump condition that $m_s m_D = 1$ where m_s and m_D are, respectively, the Mach numbers of the flow just upstream and immediately downstream of the shock) with the solution that is subsonic at $r < r_L$ and transonic at $r = r_L$. Flows corresponding to all solution curves that intersect this dashed curve must contain such a shock if they are to be steady within the mass-loading region, and to exit the mass-loading region transonically. If the pressure boundary condition at large radii is small, the outflow will follow the transonic solution; for high external pressures, the shock radius will be rather smaller and the flow will exit the mass-loading region as a subsonic "breeze." Note that the strongest central winds can blow straight through the mass-loading region without forming a shock—this is the case where equation (7b) yields $r_s > r_P$.

In Figure 2 the dotted curve shows the estimated locus of isothermal shocks, (r_s, m_s), given by equations (4b) and (11a). This compares with the "exact" numerically calculated value of m_s shown by the dashed curve in this figure. Approximate solutions for particular values of v_*, shown by open circles, are connected with the radius at which the exact solutions predict that a shock would form by a bar. The approximate locus of shocks is in reasonable agreement with the exact one, except close to the very edge of the mass region where $m \to 2$ for the

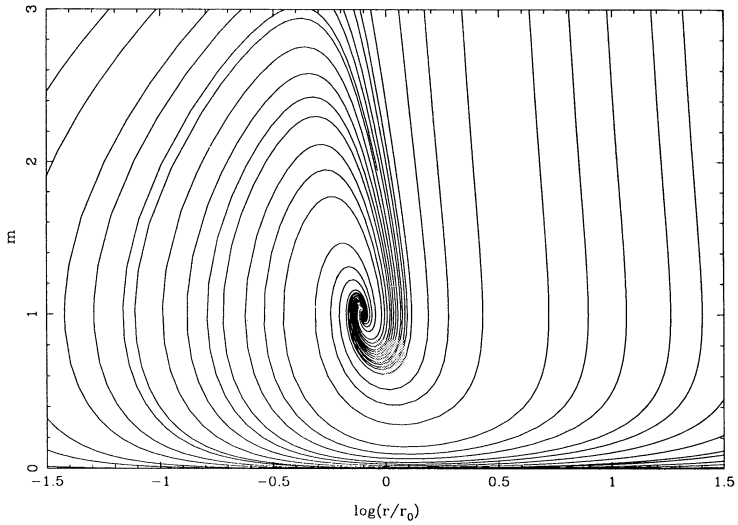

FIG. 1*a*

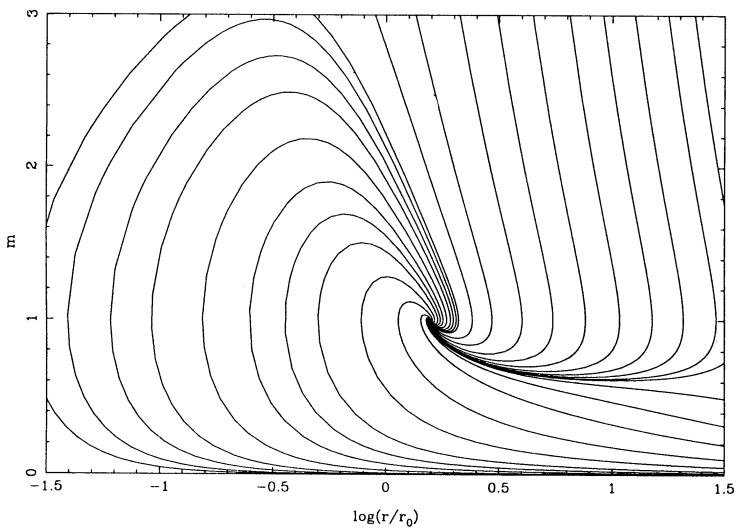

FIG. 1*b*

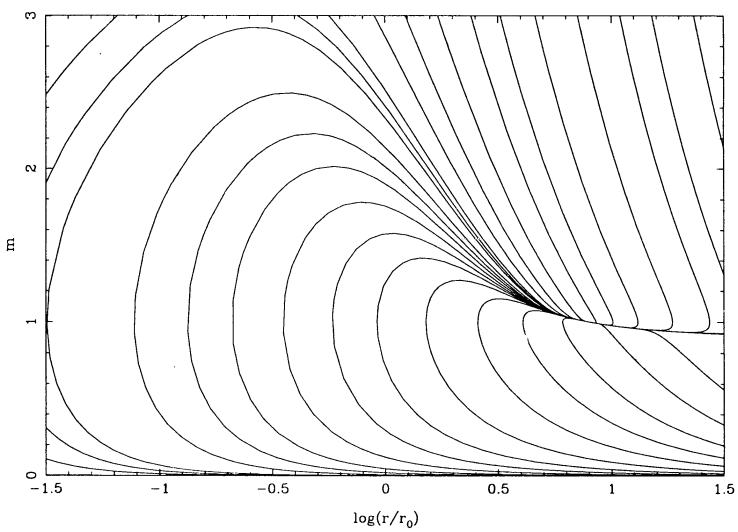

FIG. 1*c*

FIG. 1.—Solutions for infinitely extended mass-loading regions with various values of Γ. (*a*) $\Gamma = 0$; (*b*) $\Gamma = -1.5$; (*c*) $\Gamma = -1.9$.

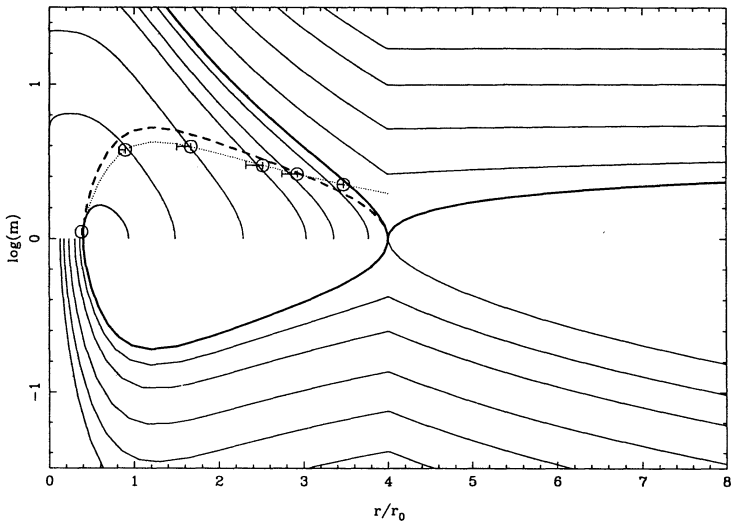

FIG. 2.—Isothermal spherical solutions for a wind blowing into a region with uniform mass-loading inside a radius $r_L = 4r_0$, and zero mass-loading beyond it. In this case, the sonic point (at $r \simeq 0.8r_0$) is a spiral. The solid curves show a range of solutions to the Mach number equation, chosen, for clarity, to terminate where the gradient of the Mach number is infinite. The bold curve shows the unique solution that is supersonic at large radii; the dashed curve shows the locus of values $m(x)$ which can pass onto the outer transonic solution through a shock. The dotted curve shows the shock strengths derived from eqs. (4b) and (11a), which provide an approximation to the dashed curve. Points for specific values of v_* are shown by open circles—bars are drawn between their centers and the numerically determined shock radii.

approximation. The individual points are perturbed from the exact shock radii by the countervailing effects of the neglect of pressure forces in equation (4a) and the assumption that $I(r) \gg \dot{M}_*$ used in deriving equation (11a).

Figure 3 shows solutions for $\Gamma = -1.77$ (which gives a nodal inner sonic point) and $r_L = 18r_0$. The plot is similar to that of Figure 2, except for the existence of singular and non-singular solutions which pass smoothly through the inner sonic point (the singular solution is shown bold in Fig. 3). Unlike a $\Gamma = 0$ mass-loading region, a $\Gamma = -1.77$ mass-loading region, with its nodal inner sonic point, can contain a wind that is supersonic at $r < r_0$ and becomes subsonic in the mass-loading region *without* passing through a shock, before emerging from the region transonically at $r = r_L$. Indeed, any solution which is below the (bold) singular solution upstream of the inner sonic point can pass smoothly onto the transonic solution. The correspondence of the approximate and "exact" shock loci (r, m) in this case are far poorer, as might be expected since the shocks which form in this case are never strong. The predictions of individual shock radii $r_s(v_*)$ are, however, still quite reasonable.

6. CONCLUSION

Clearly, mass-loaded isothermal winds often pass through global shocks at speeds that are substantially smaller than the wind speeds at the inner edges of the mass-loading regions. If

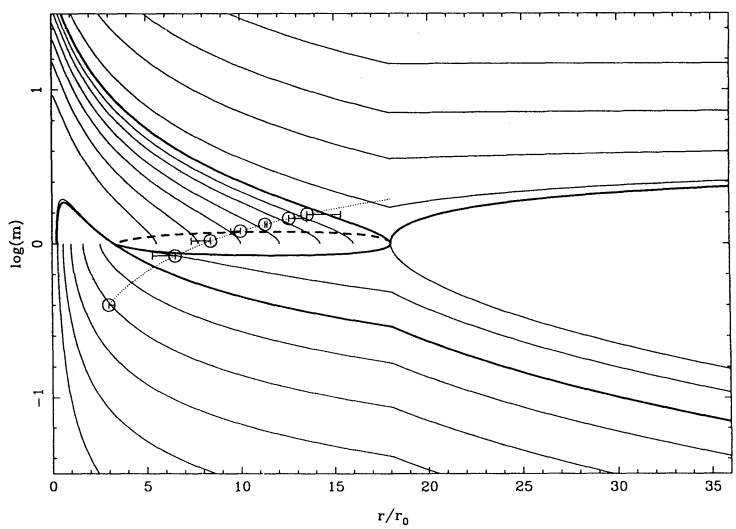

FIG. 3.—Isothermal spherical solutions for a wind blowing into a region with mass-loading index $\Gamma = -1.77$ inside a radius $r_L = 18r_0$, and zero mass-loading beyond it. In this case, the sonic point (at $r \simeq 3.3r_0$) is a node (in Fig. 2, the sonic point was a spiral). As in Fig. 2, the solid curves show a range of solutions to the Mach number equation, chosen, for clarity, to terminate where the gradient of the Mach number is infinite. One bold curve shows the unique solution that is supersonic at large radii; the dashed curve shows the locus of values $m(x)$ which can pass onto the outer transonic solution through a shock. A further bold curve, which tends to Mach zero at large radii, is the singular solution through the sonic point. The dotted curve shows the shock strengths derived from eqs. (4b) and (11a), which provide a (poor) approximation to the dashed curve. Points for specific values of v_* are shown by open circles—bars are drawn between their centers and the numerically determined shock radii.

mass entrainment occurs through gradual viscous coupling of the winds to the entrained mass, the weakness of the global shocks that do develop will certainly lead to the winds being weak sources of hard thermal emission relative to comparable shocked unloaded winds. The shocks' weakness may also have consequences for the radio loudness of some wind sources.

In closing, we address the question of whether the wind in NGC 6888 is likely to behave like an isothermal wind as it is mass loaded, since it provides an example of a wind bubble with a completely thermal radio spectrum. The wind speed and mass-loss rate in this object are 2400 km s^{-1}—roughly Mach 150 at 10^4 K—and $1.1 \times 10^{-4}\ M_\odot\ yr^{-1}$ (St. Louis et al. 1989) so that from equations (2a) and (4b) the number density of the wind is roughly

$$n_* \simeq 0.1\ \mathrm{cm}^{-3}\left(\frac{r}{1\ \mathrm{pc}}\right)^{-2}\left[1+\left(\frac{r}{r_0}\right)^{\Gamma+3}\right]^2 . \quad (23)$$

If solar abundances and collisional ionization equilibrium are assumed, the maximum value of Λ is

$$\Lambda_{\max} \simeq 1 \times 10^{-21}\ \mathrm{ergs\ cm}^{-3}\ \mathrm{s}^{-1}\left(\frac{n_*}{1\ \mathrm{cm}^{-3}}\right)^2 \quad (24)$$

(e.g., Raymond, Cox, & Smith 1976; Gaetz & Salpeter 1983) in the wind that has not undergone much mass loading; $\Lambda = \Lambda_{\max}$ at a temperature of roughly 10^5 K. Because the wind is likely to have heavy element fractional abundances greater than those in the Sun, and the ionization structure may be out of equilibrium, the value of Λ in the wind will be assumed to be greater than $\Lambda_{\max}$ by a factor f which reasonably may lie in the range of 10–100. We estimate that between $r = 0$ and $r = r_0$

$$\frac{1}{2}Sv^2 \simeq 1 \times 10^{-18}\ \mathrm{ergs\ cm}^{-3} \times \left(\frac{r_0}{1\ \mathrm{pc}}\right)^{-3}\left(1+\frac{\Gamma}{3}\right)\frac{(r/r_0)^\Gamma}{[1+(r/r_0)^{\Gamma+3}]^2} . \quad (25)$$

Using equations (23), (24), and (25) we see that the Wolf-Rayet wind is likely to behave isothermally when $\frac{1}{2}Sv^2/\Lambda_{\max} < 1$, where

$$\frac{\frac{1}{2}Sv^2}{\Lambda_{\max}} \simeq 1 \times 10^3\left(\frac{f}{100}\right)^{-1}\left(\frac{r}{1\ \mathrm{pc}}\right)\left(1+\frac{\Gamma}{3}\right)\frac{(r/r_0)^{\Gamma+3}}{[1+(r/r_0)^{\Gamma+3}]^6} . \quad (26)$$

For $\Gamma = 0$ and fixed r_0, this ratio peaks when $r/r_0 = (2/7)^{1/3} \simeq 0.66$. For $\frac{1}{2}Sv^2/\Lambda_{\max} < 1$ at all radii, we require that

$$r_0 \lesssim 2.5 \times 10^{-2}\ \mathrm{pc}\left(\frac{f}{100}\right) . \quad (27)$$

Compared to the nebular extent of several parsecs this is small. However, r_0 can be small if the Wolf-Rayet wind is mass loaded by the clumpy ejecta of a binary supergiant companion. Such a supergiant companion would probably be difficult to detect as it is clear that M3 supergiants are less luminous than the massive He emission-line stars that have been detected in the Galactic center and which are probably related to Wolf-Rayet stars (Eckart et al. 1993).

The process discussed in this paper may also have relevance for radio quietness or X-ray quietness in other types of wind-blown bubbles including, perhaps, those around compact sources at the centers of some active galactic nuclei (AGNs). For instance, the great widths of the broad absorption lines detected toward some AGNs and the relative radio quietness of those AGNs (e.g., Turnshek 1988) may be associated with the mass loading of nearly isothermal winds. While they are of lower speeds and, hence, may not be expected to be strong X-ray or radio sources, the broad H_2 line–forming regions in Orion may also be in mass loaded isothermal winds (Malone, Dyson, & Hartquist 1994).

We thank the referee for a thoughtful report, which helped us to improve the clarity and completeness of this paper.

REFERENCES

Arthur, S. J., Dyson, J. E., & Hartquist, T. W. 1993, MNRAS, 261, 425
———. 1994, MNRAS, 269, 1117
Asvarov, A. I. 1992, Soviet Astron., 36, 386
Bally, J., et al. 1989, ApJ, 338, L65
Beltrametti, M., & Perry, J. J. 1980, A&A, 82, 99
Chevalier, R., & Clegg, A. 1985, Nature, 317, 44
David, L. P., Durisen, R. H., & Cohn, H. N. 1987a, ApJ, 313, 556
———. 1987b, ApJ, 316, 505
Durisen, R. H., & Burns, J. O. 1981, MNRAS, 195, 535
Dyson, J. E., & Hartquist, T. W. 1992, Ap. Lett. Comm., 28, 301
Dyson, J. E., & Williams, R. J. R. 1995, in preparation
Eckart, A., Genzel, R., Hofmann, R., Sams, B. J., & Tacconi-Garman, L. E. 1993, ApJ, 407, L77
Ellison, D. C., & Möbius, E. 1987, ApJ, 318, 474
Gaetz, T. J., & Salpeter, E. E. 1983, ApJS, 52, 155
Hartquist, T. W., & Dyson, J. E. 1993, QJRAS, 34, 57
Hartquist, T. W., Dyson, J. E., Pettini, M., & Smith, L. J. 1986, MNRAS, 221, 715
Holzer, T. E., 1977, J. Geophys. Res., 82, 23
Kulkarni, S. R., Vogel, S. N., Wang, Z., & Wood, D. O. S. Nature, 360, 139
Leitherer, C. 1994, Rev. Mod. Astron. 7, in press
Malone, M. T., Dyson, J. E., & Hartquist, T. W. 1994, Ap&SS, 216, 143
Mathews, W. G., & Baker, J. C. 1971, ApJ, 170, 241
Meaburn, J., Nicholson, R. A., Bryce, M., Dyson, J. E., & Walsh, J. R. 1991, MNRAS, 252, 535
Ostriker, J. P., McCray, R. A., Weaver, R., & Yahil, A. 1976, ApJ, 208, L61
Parker, E. N. 1965, Space Sci. Rev., 4, 666
Poll, A. 1994, A&A, submitted
Raymond, J. C., Cox, D. P., & Smith, B. W. 1976, ApJ, 204, 290
Smith, L. J., Pettini, M., Dyson, J. E., & Hartquist, T. W. 1984, MNRAS, 211, 679
Smith, S. J. 1994, ApJ, submitted
St. Louis, N., Smith, L. J., Stevens, I. R., Willis, A. J., Garmany, C. D., & Conti, P. S. 1989, A&A, 226, 249
Turnshek, D. A. 1988, in QSO Absorption Lines: Probing the Universe, ed. J. C. Blades, D. A. Turnshek, & C. A. Norman (Cambridge: Cambridge Univ. Press), 17
Wendker, H. J., Smith, L. F., Israel, F. P., Habing, H. J., & Dickel, H. R. 1975, A&A, 42, 173
Williams, R. J. R. 1993, Ph.D. thesis, Univ. of Cambridge
Williams, R. J. R., & Dyson, J. E. 1994, MNRAS, 270, L52